High resolution CO J = 3-2 observations of L 1551: fragmentary structure in the outflowing shell

Journal Item

Astron. Astrophys. 250, 134–142 (1991)

ASTRONOMY
AND
ASTROPHYSICS

High resolution CO $J=3-2$ observations of L1551: fragmentary structure in the outflowing shell

N.D. Parker [1], Glenn J. White [1], S.S. Hayashi [2], and P.G. Williams [1]

[1] Department of Physics, Queen Mary and Westfield College, University of London, Mile End Road, London E1 4NS, UK
[2] Joint Astronomy Center, 665 Komohana Street, Hilo, HI 96720, USA

Received October 5, 1990; accepted March 1, 1991

Abstract. We present high resolution observations of the ^{12}CO $J=3-2$ emission associated with HH 102 in the L1551 molecular outflow. At low and intermediate blue-shifted velocities the emission is found in a shell which coincides with the optical reflection nebulosity from HH 102. In places, the shell appears to be unresolved, implying a width of less than ~ 0.01 pc. Within the shell several bright clumps can be identified. By combining the $J=3-2$ data with with previous $J=1-0$ maps we derive excitation temperatures and beam-filling factors for these clumps. The gas is found to be hot (up to ~ 40 K) and often has low filling factor (~ 0.2). We compare the distribution of the CO emission with those of the optical reflection nebulosity and the Hα shocked emission. The data are consistent with a fast wind from IRS 5 being shocked immediately in front of the boundary between the wind-eroded cavity and the swept-up molecular gas. We suggest that the particularly energetic activity in the vicinity of HH 102 is a result of the direct impact of material in a fast, collimated jet such as those traced by the radio jets emanating from IRS 5. If so, previous interpretations of the presence of both red- and blue-shifted CO around HH 102 may be incorrect. In particular, the data need not be explained as solely due to the presence of a slow rotation of the outflow about its axis.

Key words: interstellar medium: clouds; L1551 – interstellar medium: molecules – interstellar medium: kinematics and dynamics – Herbig-Haro objects – radius lines: molecular

1. Introduction

Observations of Carbon monoxide (CO) towards sites of recent star formation often reveal broad emission-line profiles (Zuckerman 1976; Bally & Lada 1983). These ordered and highly supersonic mass motions signify the presence of collimated, high-velocity outflowing gas associated with the young stars (Snell et al. 1984). In many cases the molecular outflows exhibit a large degree of symmetry, often showing a distinct bipolar structure (Snell et al. 1980; Lada 1985). The masses and the kinetic energies of these outflows are considerable (Margulis & Lada 1985). This, and their frequency of occurrence (Lada 1985; Myers et al. 1988; Parker 1989), suggest that outflows represent an important phase in the evolution of most, if not all, young stars. In particular, the onset of outflow activity might trigger the transition of an embedded protostar into a pre-main-sequence star via the violent disruption and dispersal of the surrounding dense core (Mathieu et al. 1988; Parker et al. 1988).

The prototypical example of a bipolar outflow is that located in the dark cloud L1551 (Snell et al. 1980). The outflow is centred on the infrared source IRS 5 (Beichman & Harris 1981) which is almost certainly the source responsible for driving the flow. The molecular outflow has associated with it several of the classical signposts of energetic wind activity. These include extensive shock-excited Hα emission (Snell et al. 1985) and more compact Herbig-Haro objects such as HH 29, which have large radial velocities directed away from IRS 5 (Cudworth & Herbig 1979). The outflow exhibits prominent collimation on all scales so far observed, from the extended molecular emission (Uchida et al. 1987) down to the small scale radio jets (Cohen et al. 1982) and optical jet features (Mundt & Fried 1983) which emanate from IRS 5. Recent high-resolution observations have shown that the molecular gas is located in a thin shell at the edge of the flow (Snell & Schloerb 1985; Rainey et al. 1987; Moriarty-Schieven et al. 1987b), though such high-resolution data are relatively rare.

In order to understand the physics of outflow processes, it is necessary to derive flow parameters such as mass and energy, and to determine the underlying flow pattern responsible for the observed kinematics. Previous observations aimed at deducing the physical parameters of the outflowing gas have all too often relied on too many assumptions regarding excitation temperature and filling factor (see Margulis & Lada 1985). This leads to large uncertainties in the estimates of the mass and kinetic energy in the flow. Some observations have been interpreted to suggest that outflowing gas is clumpy (Plambeck et al. 1983), though that conclusion has also been questioned (Canto et al. 1987). The observed structure and kinematics can lead to meaningful constraints being placed on current models of outflows. Uchida et al. (1987) claim to have found evidence for a slow rotation of the L1551 outflow around its symmetry axis. If correct, this would support models in which a hydromagnetic wind is driven off the surface of a rotating disc surrounding IRS 5 (e.g. Uchida & Shibata 1985; Pudritz & Norman 1986). However, the evidence is not altogether satisfactory and existing data may be explained in other ways. These unanswered questions illustrate the necessity of obtaining

Send offprint requests to: G.J. White

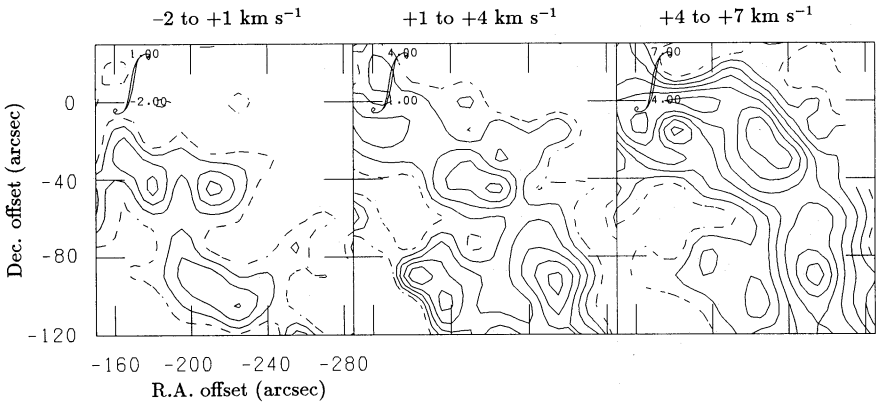

Fig. 1. Channel maps of the spatial distribution of ^{12}CO $J=3-2$ emission in the region around HH 102. Contours are integrated intensity (T_A^*) in the velocity ranges $v_{LSR} = -2$–1 km s^{-1}, 1–4 km s^{-1} and 4–7 km s^{-1}. The contour interval is 2 K km s^{-1} and the lowest contour is 3 K km s^{-1} on each of the plots. Map offsets are given relative to the position of IRS 5 (Sect. 3)

high spatial resolution observations to study, in particular, the flow processes at the interface between the wind-eroded cavity and the surrounding ambient cloud.

In this paper, we present high-resolution ^{12}CO $J=3-2$ observations of the interface in the vicinity of HH 102 in the L1551 outflow. The proximity of L1551 to the Sun ($\sim$140 pc; Elias 1978) permits the high spatial resolutions required to study the details of the structure in such regions. The data are combined with those of Uchida et al. (1987) to derive values of excitation temperature and filling factor for clumps which are resolved in the outflow shell. The observed structure is discussed in the context of its location with respect to other features in the outflow, including the orientation of the radio jets from IRS 5. Finally, we question the conclusion that the outflow is rotating.

2. Observations

The ^{12}CO $J=3-2$ data presented in this paper were obtained using the 15-m James Clerk Maxwell Telescope[1], located on Mauna Kea, Hawaii, during February 1988. The common-user 345 GHz Schottky receiver was used with an acusto-optical spectrometer backend which provided 1024 channels of (over-sampled) spectral width 0.48 MHz (effective resolution $\sim$1 MHz). At 345 GHz the telescope beamwidth was $\Theta_{beam} = 15''$. Observations were carried out in a position-switching mode with integration times of 60 s on- and 60 s off-source. Effective single-sideband system noise temperature (on-sky) were typically 2800 K, resulting in $\pm$1 rms noise in each of the spectrometer channels of 0.9 K (ΔT_A^*). The spectra and maps presented here are calibrated to the scale of T_A^* (Kutner & Ulich 1981). Conversion to T_R^* is made by dividing by the forward spillover and scattering efficiency, η_{fss}, which was determined to be $\sim$0.75. Pointing was checked regularly by observations of the planets and was found to be good to better than $\sim 5''$. Maps were made on square grids in right ascension and declination, with grid sampling $15''$ (1 beamwidth). All spectra have had linear and sinusoidal baselines removed.

[1] The James Clerk Maxwell Telescope is operated by the Royal Observatory Edinburgh on behalf of the Science and Engineering Research Council of the United Kingdom, the Netherlands Organisation for Pure Research and the National Research Council of Canada.

3. Results

The area mapped lies to the west of L1551 IRS 5 and covers most of the HH 102 region in the southwest blue-shifted outflow lobe. The essential features of the map and its location with respect to IRS 5, HH 102 and the large scale blue-shifted outflow are shown in Fig. 6 (Sect. 4). All maps presented in this paper are plotted on axes of offsets, in arcsec, from IRS 5; the coordinates of IRS 5 are taken to be RA (1950) = $04^h28^m40^s.2$, Dec (1950) = $18°01'42''$.

3.1. *Structure and geometry*

Figure 1 shows a series of channel maps of the ^{12}CO $J=3-2$ integrated intensity (T_A^*) as a function of velocity (v_{LSR}) through the blue-shifted line wing. The average velocity of the ambient cloud material is taken to be $v_{LSR} \simeq 7$ km s^{-1} and so the plots correspond to the high-velocity blue-shifted (-2 to 1 km s^{-1}), intermediate-velocity blue-shifted (1 to 4 km s^{-1}) and low velocity blue-shifted (4 to 7 km s^{-1}) gas. The figure illustrates several important features exhibited by the emission. First, there is an overall trend in the location of regions of brighter emission as a function of velocity: In the range $v_{LSR} = -2$ to 1 km s^{-1} the emission occupies predominantly the southeastern region of the map. In the range $v_{LSR} = 1$ to 4 km s^{-1} the emission is still found in the southeast but a greater proportion of it is now seen to extend further to the west and northwest. In the range $v_{LSR} = 4$ to 7 km s^{-1} one finds the emission confined to a region lying to the north and northwest of the regions previously occupied.

Second, as one moves from the high- to low-velocity blue-shifted gas the emitting region becomes better defined: For $v_{LSR} = -2$ to 1 km s^{-1} the emission originates in three separate regions. For $v_{LSR} = 1$ to 4 km s^{-1} a broad ridge running approximately northeast to southwest is becoming apparent, although within this ridge there are several regions of brighter emission. For $v_{LSR} = 4$ to 7 km s^{-1} the ridge has narrowed considerably and has become more prominently defined. It takes on the appearance of an arc, with centre of curvature to the southeast. Finally, the emission is inhomogeneous in all the velocity ranges considered. Of particular interest is the series of bright knots, or clumps, which lie roughly along the curve delineating the locus of peak emission in the ridge, as seen in the range $v_{LSR} = 4$ to 7 km s^{-1}.

The data clearly illustrate the "shell-like" structure exhibited by the low-velocity blue-shifted gas in the region of HH 102. This shell has been noted in previous studies (Snell & Schloerb 1985; Rainey et al. 1987) in which it was found that the low-velocity shell

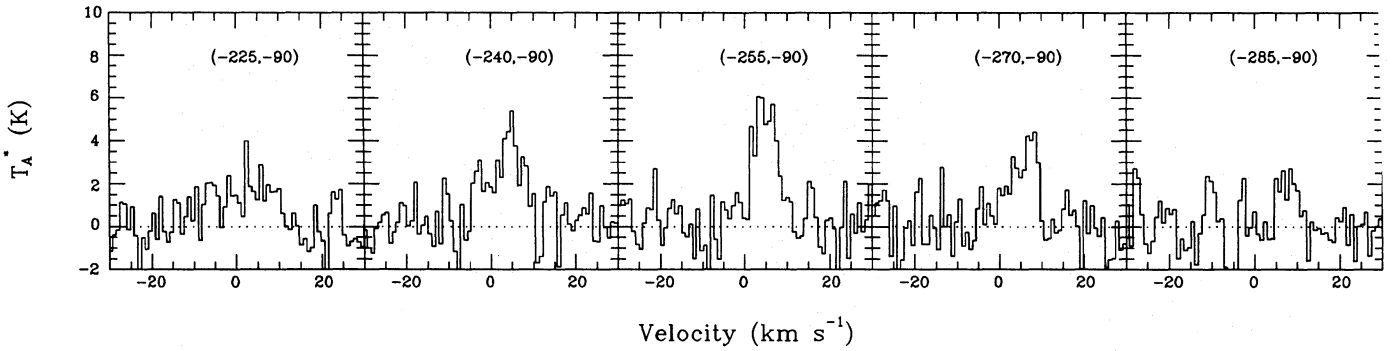

Fig. 2. The sequence of ^{12}CO $J=3-2$ spectra in the scan at constant declination through clump C. Offsets measured from the $J=3-2$ map centre, in units of arcsec, are indicated for each spectrum

is present around much of the blue-shifted outflow lobe (Moriarty-Schieven et al. 1987b). Furthermore, an analogous velocity structure is seen, though less prominently, in the red-shifted lobe (Uchida et al. 1987; Moriarty-Schieven et al. 1987b). These authors find that the shell structure is more clearly defined at low blue-shifted velocities and that it is coincident with the edge of the reflection nebula HH 102. At higher blue-shifted velocities the emission is found closer to the outflow axis (e.g. Fridlund & White 1989), the structure being of a fragmentary nature with a scale size $\sim 60''$.

The variation in line profiles across the shell is illustrated in Fig. 2. The figure shows a sequence of spectra representing a scan across the shell, with scan centre at map offset $(-255, -90)$. The spectra lie along a line of constant declination and so the scan direction is roughly perpendicular to the local shell axis. The peak antenna temperature varies considerably across the shell; at the ends of the scan one sees T_A^* (peak) ~ 2–3 K, whereas at the centre T_A^* (peak) ~ 5–7 K. From averaging several spectra not associated with the shell, the line core due to ambient gas in the L 1551 cloud is found to have $T_A^* \sim 2$ K, centroid $v_0 \sim 7$ km s^{-1} and width $\Delta v_{\rm FWHM} \sim 1.5$ km s^{-1}. Thus it would appear that the line profiles seen in the shell are almost entirely due to material with significant kinematic offset from (and perhaps higher excitation than) the ambient L1551 cloud component.

Figure 3 shows the variation of integrated intensity as a function of map offset for the row of spectra described above. In the high-velocity range ($v_{\rm LSR} = -1$ to 2 km s^{-1}) the intensity falls gradually towards the edge of the outflow and there is little evidence of a shell. In the intermediate- and low-velocity ranges the shell is well defined, with peak intensity occurring at RA offset $-255''$. A map of the spatial distribution of integrated intensity for the range $v_{\rm LSR} = 5$ to 7 km s^{-1} is presented in Fig. 4. The shell separates into a series of three clumps along the locus of peak intensity. These clumps are labelled A, B, and C in the figure. A fourth clump, labelled D, is found in the interior of the arc of the shell. Clumps A, B, and C are all of comparable brightness. They have size $\sim 20''$ and a roughly regular spacing of $\sim 55''$. Clump D is less bright (by approximately a factor of 2) and lies about $1'$ from the rest of the shell.

The observed width of the shell will be greater than its true width because of beam-smearing effects. An estimate of the true width can be obtained from a crude deconvolution;

$$\Theta_{\rm true} \simeq \sqrt{\Theta_{\rm obs}^2 - \Theta_{\rm beam}^2}\,, \qquad (1)$$

where $\Theta_{\rm obs}$ is the observed source width at half maximum and $\Theta_{\rm beam}$ is the beamwidth at half maximum. Across clump C, at

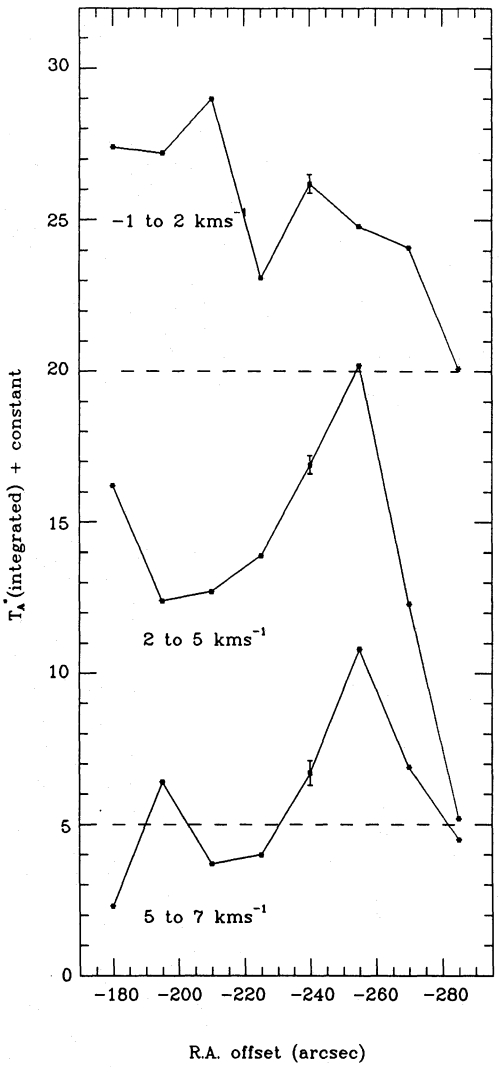

Fig. 3. The variation of ^{12}CO $J=3-2$ integrated intensities (T_A^*) as a function of RA offset at declination offset $-90''$. Three velocity ranges are shown in order to illustrate the prominence of the shell at low and intermediate blue-shifted velocities. For clarity, the plots for $v_{\rm LSR} = 2$ to 5 km s^{-1} and $v_{\rm LSR} = -1$ to 2 km s^{-1} have been offset by 5 K km s^{-1} and 20 K km s^{-1} respectively; the dashed lines indicate their proper zero levels. Errorbars correspond to $\pm 1\sigma$ rms noise in the integrated intensities for the velocity ranges considered

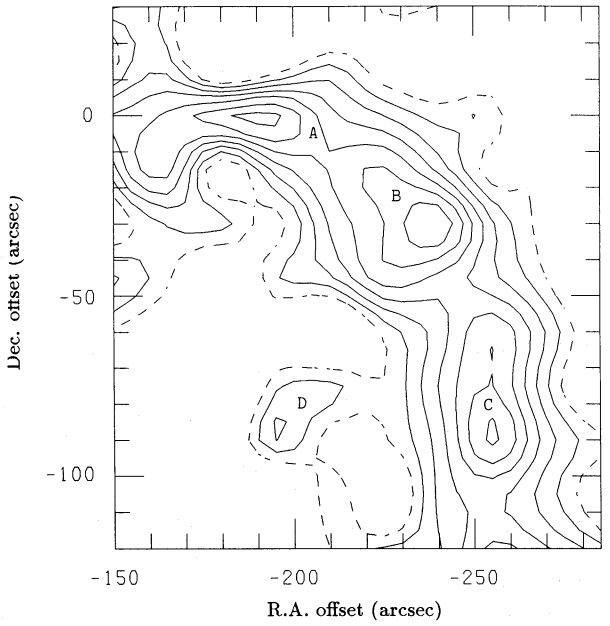

Fig. 4. Contour plot of the spatial distribution of ^{12}CO $J=3-2$ integrated intensity (T_A^*) for the velocity range $v_{LSR}=5$ to 7 km s^{-1}. The contour interval is 1 K km s^{-1} and the lowest contour is 4 K km s^{-1}. Map offsets are as for Fig. 1. Note the presence of several knots of bright emission which are labelled A, B, C, and D

declination $-90''$, the shell seen in $v_{LSR}=5$ to 7 km s^{-1} has an observed width $\Theta_{obs}\sim 30''$ (Fig. 3). Assuming $\Theta_{beam}=15''$, this leads to $\Theta_{true}\sim 25''$. Similarly, across clump B with scan position angle 135°, one finds $\Theta_{true}\sim 22''$. At the northern end of the shell, near to clump A, the shell appears somewhat narrower than this, perhaps being unresolved here. For most of the shell in the region of HH 102, however, the data suggest a shell thickness, t_{shell}, of $\sim 20-25''$. Defining

$$\Gamma=\frac{t_{shell}}{d_{flow}}, \tag{2}$$

in which d_{flow} is the outflow lobe diameter perpendicular to the local outflow symmetry axis, Γ has value typically $\lesssim 1/10$.

These high resolution observations confirm some of the predictions which have arisen from consideration of previous data obtained with larger beams. Rainey et al. (1987) used ^{12}CO $J=2-1$ observations with beamwidth $\Theta_{beam}=30''$ to place upper limits of $\sim 40''-90''$ on the width of the shell for velocities around $v_{LSR}=3.5$ km s^{-1}. A similar width ($t_{shell}\lesssim 40''$) was inferred by Snell & Schloerb (1985), although their lunar occultation measurements suggested that the shell feature was extremely narrow in places ($\lesssim 10''$). Higher resolution maps, using Maximum Entropy image reconstruction (Morarty-Schieven et al. 1987b) reveal structure similar to that seen in the present study (Moriarty-Schieven & Snell 1988; Moriarty-Schieven et al. 1987a), and similar values for Γ.

3.2. *Analysis of the ^{12}CO $J=3-2$ data*

In order to understand the physics of the processes occurring in the molecular outflow one must be able to derive values of the important parameters of the emitting gas, including excitation temperature, T_{ex}, optical depth, τ, and beam-filling factor, f. Observations of a single optically-thick transition are insufficient for determination of such parameters unless certain quantities are known. The standard analysis of CO data utilizes observations of ^{12}CO and the isotope ^{13}CO in two transitions (see e.g. Cantó et al. 1987; Margulis & Lada 1985) and generally employs the "local thermodynamic equilibrium" (LTE) approximation. The present dataset does not include any ^{13}CO spectra. However, previous observations of the 115 GHz ^{12}CO $J=1-0$ emission, with similar beam size, can be combined with the ^{12}CO $J=3-2$ data in order to estimate some of the above parameters. The ^{12}CO data are taken from the observations of Uchida et al. (1987), who used the Nobeyama Radio Observatory (NRO) 45-m telescope to map the L1551 outflow. At 115 GHz the NRO beamwidth was $\Theta_{FWHM}\simeq 16''$ and the main-beam efficiency, η_{MB}, was 0.45. We now use the observed line ratios to estimate T_{ex}.

Initially it will be assumed that the LTE approximation is valid for rotational states up to $J=3$, and that T_{ex} is constant along a given line-of sight. Thus the levels will be thermalized with $T_{ex}(3-2)=T_{ex}(1-0)=T_K$, where T_K is the gas kinetic temperature. The observed radiation temperature for the J+1 → J transition is then

$$T_R=f_{J+1}\left[\mathscr{J}_{J+1}(T_{ex})-\mathscr{J}_{J+1}(T_{bg})\right](1-e^{-\tau_{J+1}}), \tag{3}$$

where the subscript J+1 refers to the upper rotational level in question. In this expression f_{J+1} is the beam-filling factor, T_{bg} is the background temperature (~ 2.7 K for the microwave background) and τ_{J+1} is the optical depth in the transition. $\mathscr{J}_{J+1}$ is the radiation intensity and is defined by

$$\mathscr{J}_{J+1}(T)=\frac{h\nu_{J+1}}{k}\left[\frac{1}{e^{h\nu_{J+1}/kT}-1}\right]. \tag{4}$$

It is easily shown that the expression for the line ratio, $T_R(3-2)/T_R(1-0)$, simplifies considerably in two regimes: For hot, optically-thin gas one has $T_R(3-2)/T_R(1-0)\sim 9\,f_{J+1}/f_{K+1}$. In the optically-thich case, assuming negligible background contribution and that $f_{J+1}=f_{K+1}$, the temperature ratio reduces to

$$\frac{T_R(3-2)}{T_R(1-0)}=3\left[\frac{e^{h\nu_{10}/kT_{ex}}-1}{e^{3h\nu_{10}/kT_{ex}}-1}\right], \tag{5}$$

which can be solved numerically for T_{ex}. This method of investigating line ratios has the advantage that one does not require knowledge of the absolute values of the filling factors. Instead, is has been assumed simply that $f_{J+1}=f_{K+1}$, which is a less exacting and perhaps more realistic assumption. Errors introduced by this and other assumptions will be discussed towards the end of this section.

For this calculation the data have been calibrated to main-beam brightness temperatures, T_{MB}, using $\eta_{MB}(1-0)=0.45$ and $\eta_{MB}(3-2)=0.6$. Table 1 presents these data for clumps A, B, and C for the velocity range $v_{LSR}=5$ to 7 km s^{-1} (see Fig. 4). Also shown are values of $T_{MB}(3-2)/T_{MB}(1-0)$. These are somewhat less than 1 and, thus, an order of magnitude too low to be consistent with that expected for the hot, optically-thin case. This result is in agreement with previous studies of the outflow shell (Moriarty-Schieven & Snell 1988; Fridlund & White 1989), although at some locations in the "cavity" interior to the shell the ^{12}CO $J=1-0$ emission has been suggested to be optically-thin (Phillips et al 1982; Richardson et al. 1985).

More likely is the case that both the $J=3-2$ and $J=1-0$ transitions are optically-thick in the low-velocity blue-shifted shell. Figure 5 shows a plot of the ratio $R=1/3\,[T_{MB}(3-2)/$

Table 1

	Clump A	Clump B	Clump C
$\int_5^7 T_A^*(1-0)\,dv$	9.2 K km s^{-1}	9.5 K km s^{-1}	10 K km s^{-1}
$\int_5^7 T_A^*(3-2)\,dv$	10.4 K km s^{-1}	11 K km s^{-1}	10.3 K km s^{-1}
$\frac{1}{3}\frac{T_{MB}(3-2)}{T_{MB}(1-0)}$	0.28	0.29	0.26
T_{ex}	33 K	40 K	25 K

Table 2

	Clump A	Clump B	Clump C
$T_R^*(3-2)$	6.9 K	7.3 K	6.9 K
T_{ex}	33 K	40 K	25 K
$f\eta_c$	0.27	0.25	0.4

$T_{MB}(1-0)$] as a function of T_{ex} for the optically-thick case. R provides a useful indication of T_{ex} for $T_{ex} \lesssim 45$ K. Values of T_{ex} so derived are given in the final row of Table 1. These range from ~ 25 K for clump C, up to ~ 40 K for clump B.

With the estimates of T_{ex} one can derive values for the beam-filling factors. For this purpose the antenna temperatures are calibrated to the scale of T_R^* (Kutner & Ulich 1981; T_R^* is defined as the antenna temperature corrected for ohmic loss, atmospheric loss, spillover and scattering. It is as close as one can get to the source radiation temperature without knowledge of the underlying source brightness distribution.) Thus

$$f\eta_c = \frac{T_R^*}{[\mathscr{J}_\nu(T_{ex}) - \mathscr{J}_\nu(T_{bg})]\,(1-e^{-\tau})}, \tag{6}$$

where η_c is the coupling efficiency of the antenna pattern to the source brightness distribution. In practice, the terms f and η_c can not be separated observationally and so henceforth it will be their product which is taken to indicate the "beam-filling factor". For the ^{12}CO $J=3-2$ data, correction to T_R^* is achieved using

$$T_R^* = \frac{T_A^*}{\eta_{fss}}, \tag{7}$$

in which the forward spillover and scattering efficiency, η_{fss}, is ~ 0.75. Table 2 lists values of T_R^*, T_{ex} and $f\eta_c$ for clumps A, B, and C in the velocity range $v_{LSR} = 5$ to 7 km s^{-1} (assuming $\tau \gg 1$). It should be noted that the variation in T_{ex} for the clumps is relatively small, and that only a small number of clumps are sampled in the map. It is, therefore, not clear that a real statistical significance should be attached to the resulting variations in the derived physical parameters. What would appear to be significant is that in all cases the beam-filling factors are considerably less than 1.

It is appropriate, at this stage, to mention the sources of error in the estimates of T_{ex} and $f\eta_c$. Errors introduced by the intrinsic noise come predominantly from the $J=3-2$ data The $\pm 1\sigma$ rms deviation in integrated intensity in channels of width 2 km s^{-1} is ~ 1 K km s^{-1}, i.e. about 10% of the values of $\int T_A^*\,dv$ being considered. It was assumed that the $J=3-2$ and $J=1-0$ transitions were both optically-thick. At some positions in the outflow the $J=1-0$ emission has been suggested to be optically-thin (Phillips et al. 1982; Richardson et al. 1985). If this were the case at the map positions considered above, the value of T_{ex} would be an underestimate. As a result, the filling factors would, in reality, be even less than those derived. The assumption that $f_{3-2} = f_{1-0}$ might also be invalid, for example if the $J=3-2$ emission originates from a smaller volume than the $J=1-0$ (Richardson et al. 1985). In this case the value of T_{ex} would again be an underestimate. This effect is coupled to the more important problem of non-LTE effects which generally revolve around sub-

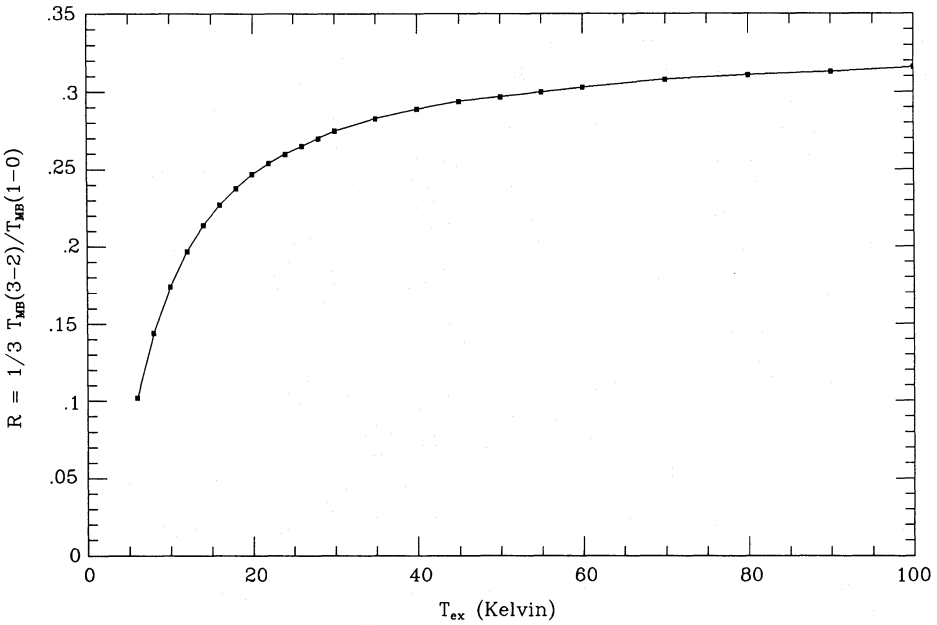

Fig. 5. Illustration of the relationship between the ratio of the ^{12}CO $J=3-2$ and $J=1-0$ radiation temperatures and the implied excitation temperature, as discussed in Sect. 3.2. The plot is for the optically-thick case under the assumption of LTE

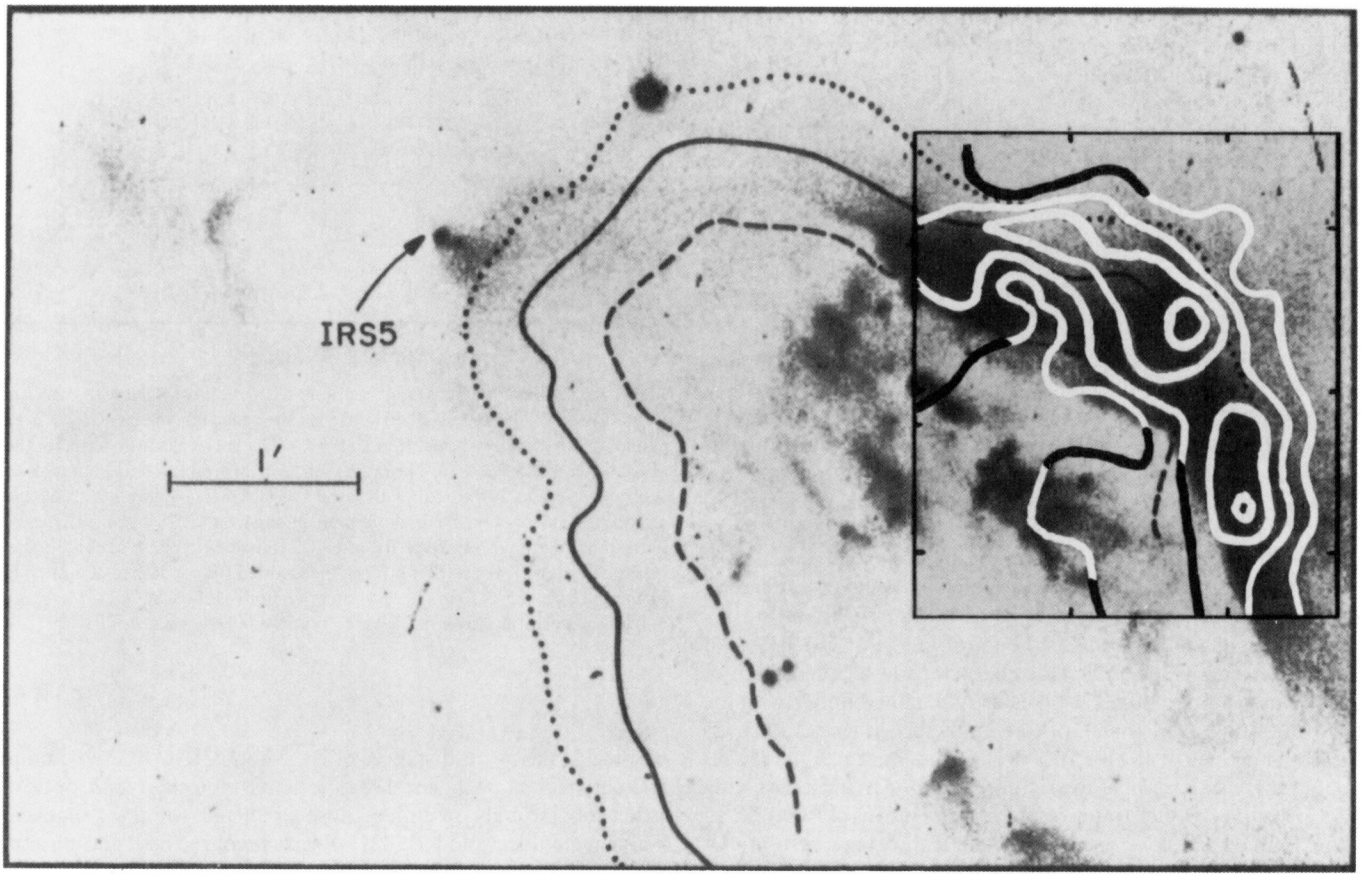

Fig. 6. The distribution of low-velocity (5–7 km s^{-1}) blue-shifted ^{12}CO $J=3-2$ emission shown in the context of its location relative to other features in the L1551 outflow. The figure comprises three sets of data: First, the underlying optical plate is an *I*-band CCD image of the region (from Moriarty-Schieven et al. 1987b). Second, the ^{12}CO $J=3-2$ map and map boundary superposed on the CCD image. The details of the contour plot are exactly as in Fig. 4, except that only every other contour is plotted here. Third, the contours external to the $J=3-2$ map are the loci of the peak intensity (solid) and half-power widths (dotted and dashed) of the low-velocity blue-shifted shell seen in the ^{12}CO $J=1-0$ data of Moriarty-Schieven et al. (1987b)

thermal excitation, variations in T_{ex} along lines-of-sight, and bulk motions (Goldreich & Kwan 1974). For example, the low densities required to thermalize the $J=1-0$ transition [$n(H_2) \gtrsim 10^3$ cm^{-3}] are not necessarily sufficient to thermalize the $J=3-2$ [$n(H_2) \gtrsim 10^4$ cm^{-3} required]. Consequently, the assumption that $T_{ex}(3-2) = T_{ex}(1-0)$ would be invalid. For a more complete discussion of non-LTE effects see Myers et al. (1983, and references therein).

4. Discussion

Figure 6 shows the observed structure of the low-velocity blue-shifted emission in the context of its location with respect to other larger scale features in the L1551 outflow. The *I*-band CCD image (from Moriarty-Schieven et al. 1987b) shows the prominent optical emission feature HH 102, which takes the form of an extended ridge running from northeast to southwest. There are also several other knots of optical emission to the southeast of HH 102. The figure also shows the loci of the peak intensity and half-power widths of the blue-shifted shell observed by Moriarty-Schieven et al. (1987b). The coincidence, in projection, of the thin limb of CO $J=3-2$ emission with the scattered optical light (see below) is further evidence in favour of a shell structure, and suggests that both delineate the interface between the excavated cavity and the surrounding dense ambient cloud.

The higher values of T_{ex} obtained using smaller beams suggests that there is still considerable structure on scales smaller than the beams (Rainey et al. 1987; Phillips et al. 1982). Such fragmentary models have been invoked to explain the variations in line profiles of the low-J transitions over the extent of the outflow (Fridlund 1987; Fridlund & White 1989). It is possible that temperature variations along the line-of sight could mimic line ratios characteristic of beam-filling factors down to ~ 0.5, even if the gas is essentially uniform (Cantó et al. 1987). Nevertheless, with such a thin shell it is unlikely that sufficient temperature variations of the type required to yield very low filling factors exist along the lines-of-sight considered. The volume filling factor is correspondingly less since it is proportional to $f^{3/2}$. The results are thus further evidence for the clumpy structure of the outflowing gas on scales smaller than $\sim 15''$; i.e. smaller than ~ 0.01 pc assuming a distance of 140 pc to L1551 (Cohen & Kuhi 1979). The emergent picture of the blue-shifted outflow at low velocities is one of a thin shell comprising a moderately hot clumpy structure on small scales.

Estimates of the outflow mass and energy will be influenced considerably by uncertainties in excitation temperature. Moriarty-Schieven & Snell (1988) examined the dependence of derved outflow mass on assumed T_{ex} and found the mass for

$T_{ex} = 35$ K to be a factor of 2 greater than that for 15 K. Of the excitation temperatures considered by Moriarty-Schieven & Snell, $T_{ex} = 35$ is in closest agreement with the values derived here, which supports their suggestion that the outflow mass and energy have previously been underestimated. For a momentum-conserving flow, in which a fast (~ 200 km s^{-1}) neutral wind sweeps up the molecular material in the shell (Bally & Lada 1983; Kwok & Volk 1985), the mass of the wind and the shell are related by

$$M_{wind} = \left(\frac{V_{shell}}{V_{wind}}\right)^2 M_{shell}, \quad (8)$$

in which V_{shell} and V_{wind} are the shell and wind velocities respectively. Snell et al. (1985) used the CO data of Snell & Schloerb (1985) to derive $M_{wind} \simeq 0.01\ M_\odot$, whereas direct observations of H I have been used to infer $M_{wind} \simeq 0.04\ M_\odot$ (Mirabel et al. (1983). [In fact, the H I observations were of the red-shifted wind but, in any case, the data of Snell & Schloerb (1985) suggest equal CO mass in the red- and blue-shifted lobes.] The low value of M_{wind} derived from the CO data might then be explained, in part, by the underestimate of M_{shell}, although the strong dependence of M_{wind} on V_{shell}/V_{wind} should also be noted.

The *I*-band filters used for the CCD image in Fig. 6 do not cover wavelengths which include characteristic shocked features usually associated with HH-objects. A narrow-band Hα frame (also admitting [N II] λ6584) of essentially the same area of sky is presented in Snell et al. (1985). The Hα emission traces the shock-excited gas, which is found to originate in many small clumps lying interior to the CO shell (interior in this sense means closer to IRS 5 along lines on the sky from IRS 5 to the features in question). Of particular interest are the relative locations of the ^{12}CO $J=3-2$ peaks, the *I*-band (reflection) and Hα (shocked) emission. The locus of peak intensity in the CO $J=3-2$ shell generally lies towards the outside (exterior) odge of HH 102 as seen in *I*-band emission. This is particularly noticeable around clumps A and B. The Hα emission lies interior to both the *I*-band and CO $J=3-2$. If the HH 102 region is delineating the cavity – ambient cloud interface then the observed geometry can be interpreted as the high-velocity wind being shocked towards the boundary of the cavity, with the reflected light from IRS 5 coming from the front surface of the swept-up shell lying immediately behind it.

Clump D lies closer to the outflow axis, not being associated with the CO $J=3-2$ shell in the same way as clumps A, B, and C. Again, the *I*-band and Hα emission lie on the side of clump D nearest to IRS 5. There are two probable suggestions for the nature of this clump. First,it could be some remnant part of the shell which happens to lie projected more towards the centre of the outflow, though in reality it lies on the edge of the cavity. Second, it could lie within the cavity, with the Hα emission arising from direct shocking by the fast neutral wind. The structure would then resemble that seen towards Herbig-Haro objects in the L1551 flow such as HH 29 (Cudworth & Herbig 1979).

In a study of HH 7–11, Rudolph & Welch (1988) found that dense clumps of gas seen in HCO^+ $J=1-0$ emission are associated with the HH objects and, furthermore, lie immediately *downwind* of the Hα emission knots (the outflow source being SVS 13; see Strom et al. 1976). Clump D exhibits the same geometry and, like the HCO^+ clumps in HH 7–11, is found at low velocity with respect to the ambient gas in the cloud ($|v - v_{amb}| \sim 1$ km s^{-1}). HH 7–11 lie in the molecular cloud associated with NGC 1333, at a distance of ~ 350–500 pc from the Sun (Lada 1985; Rudolph & Welch 1988). The (angular) separations of the clumps and Hα emission then correspond to similar

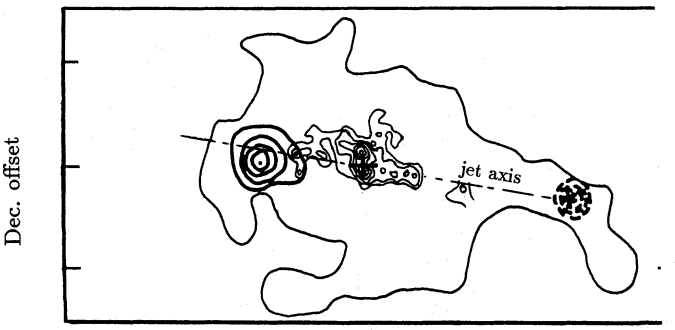

Fig. 7. Contours of the 2 cm radio continuum emission observed with the VLA by Rodriguez (1987) overlayed on a map showing the high-velocity CS $J=2-1$ clumps (from Mariarty-Schieven et al. 1987a). The axes scales are correct for the CS data, with IRS 5 at (0,0). The radio map is on an arbitrary scale, but with its centre and orientation correct with respect to IRS 5. The figure illustrates the striking alignment of the fain radio jets emanating from IRS 5 with the CS peaks in the molecular outflow. The red-shifted CS emission (thick, solid contours) is integrated over 8–10 km s^{-1} while the blue-shifted (thick, dashed contours) is integrated over 3.5–5.5 km s^{-1}. The outer contour is the CS $J=2-1$ average antenna temperature (over 5.5–8 km s^{-1}) at the 0.3 K level

physical scales at the distances of L1551 and NGC 1333. If clump D is associated with an HH object, its molecular and optical structures strongly resemble those predicted for the "shocked ambient cloudlet" model of HH objects favoured by Rudolph and Welch.

The HH 102 region exhibits features which suggest unusually strong interaction of the wind from IRS 5 with the surrounding molecular material. The bright CO $J=3-2$ peaks in the maps presented here are also seen in the high resolution ^{12}CO $J=1-0$ observations of Moriarty-Schieven et al. (1987a, b), with this emission being the brightest seen in the low-velocity blue-shifted shell. Regions of unusually large velocity dispersion (Uchida et al. 1987) are found to be coincident with two compact dense clumps of high-velocity CS emission (Snell & Schloerb 1985). These clumps lie diametrically opposite each other on a line through IRS 5; one in the northern limb of the blue-shifted lobe and the other in the southern limb of the red-shifted lobe. Both the high-velocity CS clumps are coincident with the peaks in the ^{12}CO $J=1-0$ emission and the $J=3-2$ emission presented here.

More striking still are the orientations of the optical jet features (Mundt & Fried 1983) and radio continuum jets (Rodriguez 1987) emanating from IRS 5. Figure 7 shows the spatial distribution of the CS high-velocity emission together with a VLA map of the 2 cm radio continuum emission (data from Snell & Schloerb 1985; Rodriguez 1987, respectively). The radio continuum map shows a bright double source in the immediate vicinity of IRS 5 which is interpreted by Rodriguez to be the hot inner boundary of the disc observed in the infrared by Strom et al. (1985). Emanating from the double structure are two faint radio "jets" which seem to extend to ~ 100 AU from IRS 5 (the CS $J=2-1$ and 2 cm radio contour maps are plotted on very different scales but it is only the orientations of the features which are important here). The radio jets and optical jet features are *not* aligned along the symmetry axis of the outflow, but instead project *directly* towards the high-velocity CS clumps and the peaks in the low-velocity CO shell. The peculiarly energetic activity in the region of HH 102 can then be explained in terms of the direct

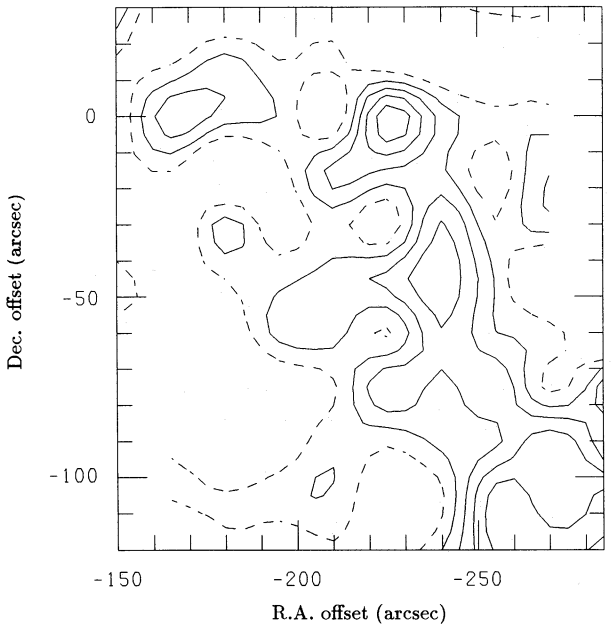

Fig. 8. The distribution of red-shifted (7–10 km s^{-1}) ^{12}CO $J=3-2$ emission in the vicinity of HH 102. Details of the map are as for Fig. 1. Contours of integrated intensity have interval 1 K km s^{-1}, with lowest contour 6 K km s^{-1}

interaction of a fast jet with the stationary ambient gas at the edge of the cavity.

Uchida et al. (1987) have noted the presence of red-shifted CO emission along the northern limb of the blue-shifted outflow lobe and blue-shifted emission along the southern limb of the red-shifted lobe. They interpret this as evidence for a large scale slow rotation of the outflow, as is predicted in the hydromagnetic outflow models of Uchida & Shibata (1985) and Pudritz & Norman (1986). The CO $J=3-2$ data presented here also reveal low-velocity red-shifted gas near to HH 102. Figure 8 shows a contour plot of the distribution of this emission in the velocity range $v_{LSR}=7$ to 10 km s^{-1}. The red-shifted gas lies along a ridge running roughly north-south and is found to lie behind a similar ridge of Hα emission. (The confusion at the southwest corner of the map is due to a few poorly calibrated spectra.)

This emission is at the same location as the peak of the red-shifted emission near HH 102 seen by Uchida et al. (1987). In view of the above discussion concerning the peculiar energetic activity in the vicinity, this red-shifted emission need not necessarily be a signature of rotation. Instead, the data could be explained as arising from the oblique impact of a high-velocity jet with the ambient material at the boundary of the cavity. Subsequent "splaying-out" of the flow after the impact, and viscous entrainment of the surrounding gas (e.g. Dyson et al. 1988), would lead to some CO with red-shifted velocities. The relatively small component of red-shifted gas is a result of the symmetry axis of the blue-shifted outflow lobe being projected out of the plane of the sky from IRS 5. Exactly the same arguments apply to the analogous region on the opposite side of IRS 5, in the southern limb of the blue-shifted outflow lobe.

5. Conclusions

We have presented high angular resolution observations of the ^{12}CO $J=3-2$ emission associated with HH 102 in the L1551 molecular outflow. The data clearly illustrate the presence of the shell feature suggested to be present in previous observations of the low- and intermediate-velocity blue-shifted gas. The shell is found to contain several clumps of bright emission which have size $\sim 20''-25''$, similar to the width of the shell over much of the area mapped. In places, however, the shell may still be unresolved, suggesting a width of $\lesssim 0.01$ pc.

By combining the $J=3-2$ data with $J=1-0$ maps made with similar beamwidth, we have investigated some of the properties of these clumps. The line ratios do not appear to be consistent with those expected for the hot optically-thin case. In the optically-thick regime we derive excitation temperatures up to ~ 40 K and beam-filling factors as low as ~ 0.2. The resulting picture of the low-velocity flow is one of a thin shell comprising numerous moderately hot, optically-thick clumps on scales less than $\sim 15''$. These data alone are not sufficient to distinguish between this limb-brightening being a column density enhancement or an excitation temperature effect.

The structure seen in the CO $J=3-2$ and optical emission can be explained by a fast wind being shocked just inside the boundary between a wind-eroded cavity and the surrounding ambient gas. The swept-up shell of CO lies immediately outside this boundary and it is the front surface of this gas which is responsible for the reflection of light from IRS 5. The location of the CO clumps with respect to shock-excited knots of Hα emission strongly resembles that seen in HH 7–11, in which the dense clumps of gas lie immediately *downwind* of the Hα emission. In the case of Herbig-Haro objects, such geometry would support "shocked ambient cloudlet" models as opposed to "bullets" ejected from IRS 5.

Bright CO and CS peaks, large velocity dispersions and shock-excited gas suggest particularly energetic activity in the vicinity of HH 102. In particular, we note the alignment of radio jets emanating from IRS 5 with the CO peaks and high-velocity clumps. Analogous structure is seen symmetrically opposite IRS 5, in the red-shifted outflow lobe. We suggest that this energetic activity can be explained in terms of the direct impact of material in the fast, collimated jet with the cavity wall at HH 102. The recent discovery of very high-velocity optical features supports this hypothesis. Subsequent "splaying-out" of material after the oblique impact would then explain the presence of both red- and blue-shifted gas at these two locations. Thus, their previous interpretation as evidence for rotation of the outflow may not necessarily be valid.

Acknowledgements. GJW and PGW thank the SERC for travel funds for the $J=3-2$ observations.

References

Bally J., Lada C.J., 1983, ApJ 265, 824
Beichman C., Harris S., 1981, ApJ 245, 589
Cantó J., Rodriguez L.F., Anglada G., 1987, ApJ 321, 877
Cohen M., Bieging J.H., Schwartz P., 1982, ApJ 253, 707
Cohen M., Kuhi L.V., 1979, ApJS 41, 743
Cudworth K.M., Herbig G.H., 1979, AJ 84, 548
Dyson J.E., Cantó J., Rodriguez L.F., 1988, Mass Outflows From Stars and Galactic Nuclei, eds. L. Bianchi, R. Gilmozzi Kluwer, London
Elias J.H., 1978, ApJ 224, 453
Fridlund C.V.M., 1987, Ph.D. Thesis, University of Stockholm
Fridlund C.V.M., White G.J., 1989, A&A 223, L13
Goldreich P., Kwan J., 1974, ApJ 189, 441

Kutner M.L., Ulich B.L., 1981, ApJ 250, 341
Kwok S., Volk K., 1985, ApJ 299, 191
Lada C.J., 1985, ARA&A 23, 267
Margulis M., Lada C.J., 1985, ApJ 299, 925
Mathieu R.D., Benson P.J., Fuller G.A., Myers P.C., Schild R.E., 1988, ApJ 330, 385
Mirabel I.F., Cantó J., Rodriguez L.F., 1983, Rev. Mex. Astron. Astrofis. 7, 235
Moriarty-Schieven G.H., Snell R.L., 1988, ApJ 332, 364
Moriarty-Schieven G.H., Snell R.L., Strom S.E., Grasdalen G.L., 1987a, ApJ 317, L95
Moriarty-Schieven G.H., Snell R.L., Strom S.E., Schloerb F.P., Strom K.M., Grasdalen G.L., 1987b, ApJ 319, 742
Mundt R., Fried J.W., 1983, ApJ 274, L83
Myers P.C., Heyer M., Snell R.L., Goldsmith P.F., 1988, ApJ 324, 907
Myers P.C., Linke R.A., Benson P.J., 1983, ApJ 264, 517
Parker N.D., 1989, Ph.D. Thesis, University of Cambridge
Parker N.D., Padman R., Scott P.F., Hills R.E., 1988, MNRAS 234, 67p
Phillips J.P., White G.J., Ade P.A.R., Cunningham C.T., Richardson K.J., Robson E.I., Watt G.D., 1982, A&A 116, 130
Plambeck R.L., Snell R.L., Loren R.B., 1983, ApJ 266, 321
Pudritz R.E., Norman C.A., 1986, ApJ 301, 571
Rainey R., White G.J., Richardson K.J., Griffin M.J., Cronin N.J., Monteiro T.S., Hilton J., 1987, A&A 179, 237
Richardson K.J., White G.J., Avery L.W., Lesurf J.C.G., Harten R.H., 1985, ApJ 290, 637
Rodriguez L.F., 1987, Star Forming Regions, IAU Symp. 115, eds. M. Peimbert, J. Jugaku, Reidel, Dordrecht
Rudolph A., Welch W.J., 1988, ApJ 326, L31
Snell R.L., Bally J., Strom S.E., Strom K.M., 1985, ApJ 290, 587
Snell R.L., Loren R.B., Plambeck R.L., 1980, ApJ 239, L17
Snell R.L., Schloerb F.P., 1985, ApJ 295, 490
Snell R.L., Scoville N.Z., Sanders D.B., Erickson N.R., 1984, ApJ 284, 176
Strom S.E., Strom K.M., Grasdalen G.L., Capps R.W., Thompson R., de Anne T., 1985, AJ 90, 2575
Strom S.E., Vrba F.J., Strom K.M., 1976, AJ 81, 314
Uchida Y., Kaifu N., Shibata K., Hayashi S.S., Hasegawa T., 1987, Star Forming Regions, IAU Symp. 115, eds. M. Peimbert, J. Jugaku, Reidel, Dordrecht
Uchida Y., Shibata K., 1985, PASJ 37, 515
Zuckerman B., Kuiper T.B.H., Rodriguez-Kuiper E.N., 1976, ApJ 209, L137